NANO · MICRO small
www.small-journal.com

Check for updates

A Gyroscope Nanogenerator with Frequency Up-Conversion Effect for Fitness and Energy Harvesting

Yansong Gai, Yuan Bai, Yu Cao, Engui Wang, Jiangtao Xue, Xuecheng Qu, Zhuo Liu, Dan Luo, and Zhou Li**

Converting the mechanical energy of human motion into electricity is considered an ideal energy supply solution for portable electronics. However, low-frequency human movement limits conversion efficiency of conventional energy harvesting devices, which is difficult to provide sustainable power for portable electronic devices. Herein, a fitness gyroscope nanogenerator (fg-NG) based on a triboelectric nanogenerator (TENG) and electromagnetic generator (EMG) is developed that can convert low-frequency wrist motion into high-frequency rotation by using the frequency up-conversion effect of the gyroscope. Remarkably, the fg-NG can reach a rotational speed of over 8000 rpm by hand, increasing the frequency by more than 280 times. The fg-NG can continuously and stably output a current of 17 mA and a voltage of 70 V at frequency of 220–230 Hz. The fg-NG is demonstrated to consistently power a hygrothermograph, smart bracelet, and mobile phone. Also, it can be applicated to a self-powered intelligent training system, showing its immense application potential in portable electronics and wireless Internet of Things devices.

1. Introduction

With the development of information technology and artificial intelligence technology, portable and wearable electronic devices are flooding into our lives and revolutionizing the way we live.[1,2] With the support of cloud computing, big data and other technologies, portable and wearable electronic devices are interconnected to form mobile sensor networks that seamlessly involve humans into the Internet of Things (IoTs).[3,4] Faced with the vast amounts of distributed sensors and electronic devices in IoTs, the conventional power supply methods based on grid and batteries may be difficult to meet their demands of lightness, convenience, wireless, and environmental friendliness.[5–7] The further development of the IoTs urgently requires the development of sustainable and renewable distributed energy to cope with the constraints of conventional power supply.[8,9] Thus, harvesting energy from surrounding environment such as solar,[10–12] thermal,[13–15] mechanical,[16–19] and biological energy,[20–22] has been considered an ideal solution. Among them, mechanical energy harvesting would be the most promising method of power generation, which is almost unaffected by external environmental conditions.[23,24]

Triboelectric nanogenerator (TENG) based on the coupling effect of triboelectrification and electrostatic induction can convert mechanical energy in the environment into electrical energy effectively.[25] Owing to the merits of lightweight, low

Y. Gai, Y. Bai, Y. Cao, E. Wang, J. Xue, X. Qu, Z. Liu, D. Luo, Z. Li
Beijing Key Laboratory of Micro-nano Energy and Sensor
Beijing Institute of Nanoenergy and Nanosystems
Chinese Academy of Sciences
Beijing 101400, China
E-mail: luodan@binn.cas.cn; zli@binn.cas.cn

Y. Gai, Z. Li
School of Chemistry and Chemical Engineering
Center on Nanoenergy Research
Guangxi University
Nanning 530004, China

Y. Bai, Y. Cao, E. Wang, Z. Li
Center on Nanoenergy Research
School of Physical Science and Technology
Guangxi University
Nanning 530004, China

The ORCID identification number(s) for the author(s) of this article can be found under https://doi.org/10.1002/smll.202108091.

J. Xue
Institute of Engineering Medicine
Beijing Institute of Technology
Beijing 100049, China

Z. Liu
Key Laboratory of Biomechanics and Mechanobiology
Ministry of Education
Beijing Advanced Innovation Center for Biomedical Engineering
School of Biological Science and Medical Engineering
Beihang University
Beijing 100083, China

Z. Li
School of Nanoscience and Technology
University of Chinese Academy of Sciences
Beijing 100049, China

Z. Li
Institute for Stem Cell and Regeneration
Chinese Academy of Sciences
Beijing 100101, China

DOI: 10.1002/smll.202108091

© 2022 Wiley-VCH GmbH

cost, easy fabrication, high conversion efficiency, TENG have been quickly developed in the field of mechanical energy harvesting, such as mechanical vibrations, ocean waves, winds and human motions.[26–29] Although great efforts have been made to improve the output performance of TENG, its low output power still makes it hardly to provide a stable and continuous electricity supply for electronics with high power demands.[7,30] TENG show the characteristics of high output voltage and low current, while the traditional electromagnetic generator (EMG) is just complementary to TENG and exhibits a low output voltage and high current under the same situation.[31,32] Therefore, hybridizing TENGs and EMGs help to significantly improve their output performance in various applications.

Converting the mechanical energy of human motion into electricity is considered an ideal energy supply solution for portable electronics.[33,34] However, humans move at a lower frequency, around 1–5 Hz. At such a low frequency, it is difficult for EMG to work effectively.[35] Even for TENG, which is good at harvesting low-frequency mechanical energy, the output energy per unit time of the device is lower than the expected practical value at a low operating frequency.[26] Therefore, it is necessary to develop the frequency up-conversion mechanisms to convert low frequency motions into high frequency motions and promote the utilization of low frequency mechanical energy.

Here, we reported a fitness gyroscope nanogenerator (fg-NG), which can effectively harvest the mechanical energy of low frequency human movements to charge batteries and power portable electronics on its own. The fg-NG consists of a gyroscope frequency up-conversion equipment, a TENG with radial grating disk structure, a disk EMG, a power management module and a USB type-C outlet. The gyroscope frequency up-conversion equipment can convert low-frequency wrist motion into high-frequency rotation. The internal flywheel of gyroscope can exceed 8000 rpm with hand drive, increasing the frequency by more than 280 times. The TENG and EMG are integrated inside the flywheel to convert the mechanical energy of high-speed rotation of the flywheel into electrical energy. The harvested energy is processed by the power management module and converted into a direct current (DC) that can be used directly through USB type-C outlet. The fg-NG can continuously and stably output a DC current of 17 mA and a DC voltage of 70 V at frequency of 220–230 Hz. The average power of TENG and EMG at the frequency of 220–230 Hz are 70 μW and 7.8 mW, respectively. To verify the feasibility of the fg-NG as the reliable instant power unit, it was used to power wearable electronics, such as hygrothermograph, smart bracelet, mobile phone. Also, it can be applicated to a self-powered intelligent training system. Therefore, our research work proposes a strategy to effectively harvest the mechanical energy of low frequency human motion through frequency up-conversion, but also presents a reliable and universal power unit for wearable electronics and wireless IoT devices.

2. Experimental Section

2.1. Fabrication of the Hybrid Nanogenerator

The TENG was manufactured by PCB technique, including a disc shaped stator and rotator. The stator ($Ø_{outer}$ = 30 mm, $Ø_{inner}$ = 7.5 mm) of TENG has two groups of patterned copper sectors as the electrodes. A 60 μm-thick nylon film was covered on the copper electrodes as the positive triboelectric layer. The rotator ($Ø_{outer}$ = 30 mm, $Ø_{inner}$ = 4 mm) of TENG has four independent copper sectors, each of which was coated with an equally shaped PTFE film (300 μm in thickness) as the negative triboelectric layer. The size of the stator and rotator of the EMG is the same as TENG. The 5 mm-thick acrylic sheet was tailored by a laser cutter as stator and rotator. Four copper coils ($Ø_{outer}$ = 10 mm, $Ø_{inner}$ = 1 mm, 5 mm in thickness) and four magnets (N52, Ø = 10 mm, 5 mm in thickness) were mounted on the stator and rotor, respectively. The copper coil was made of copper wire with a diameter of 0.08 mm. For the hybrid nanogenerator, the stators and rotators of TENG and EMG were pasted together respectively.

2.2. Characterization and Measurements

The SEM images of PTFE and nylon film were obtained by the field emission scanning electron microscope (SEM, Hitachi SU8020). The open-circuit voltage and short-circuit current were measured by an electrometer (Keithley 6517) with an oscilloscope (Teledyne LeCroy HDO 8108A).

3. Results and Discussion

The basic schematic structure of the fg-NG is illustrated in **Figure 1**a. The fg-NG mainly consists of two parts: the gyroscope frequency up-conversion equipment and the hybrid nanogenerator. The gyroscope device has two hemispherical shells, which can form a horizontal circular groove after meshing. The metal flywheel is mounted on a shaft that provides a spin axis for the flywheel. Two reduced ends of the shaft are mounted in notches of a low-friction guide ring, which is disposed in a groove of the shell and moves with the shaft and flywheel. The diameter of the reduced shaft ends is larger than the thickness of the guide ring, but slightly smaller than the width of groove. The shaft and guide ring are thereby rotate circularly within the groove. Thus, the flywheel can rotate about the spin axis (first axis) and also about the axis of the rotation of the guide ring (second axis) which is perpendicular to and intersects the spin axis. The clockwork is installed at one end of the guide ring to provide an initial spin to the flywheel. After the flywheel rotates, twist the gyroscope by hand to give it a torque on the third axis that is perpendicular to both the first and second axis. The flywheel will precess about the second axis and generate a torque opposing the manually applied torque. When the manually gyrate direction is the same as the precession direction of the flywheel, a continuous torque will be applied to the spin axis. In theory, the greater the torque applied, the faster the flywheel rotates around its spin axis.

The rotator of the hybrid nanogenerator is mounted on the flywheel and rotates with the flywheel about the spin axis. The stator is installed at the other end of the guide ring and is relatively stationary with the rotating rotator. In order to lead out the electricity generated by the hybrid nanogenerator, a conductive ring made of copper is installed in the groove. The magnets and copper coils are mounted on a laser-cut circular acrylic

© 2022 Wiley-VCH GmbH

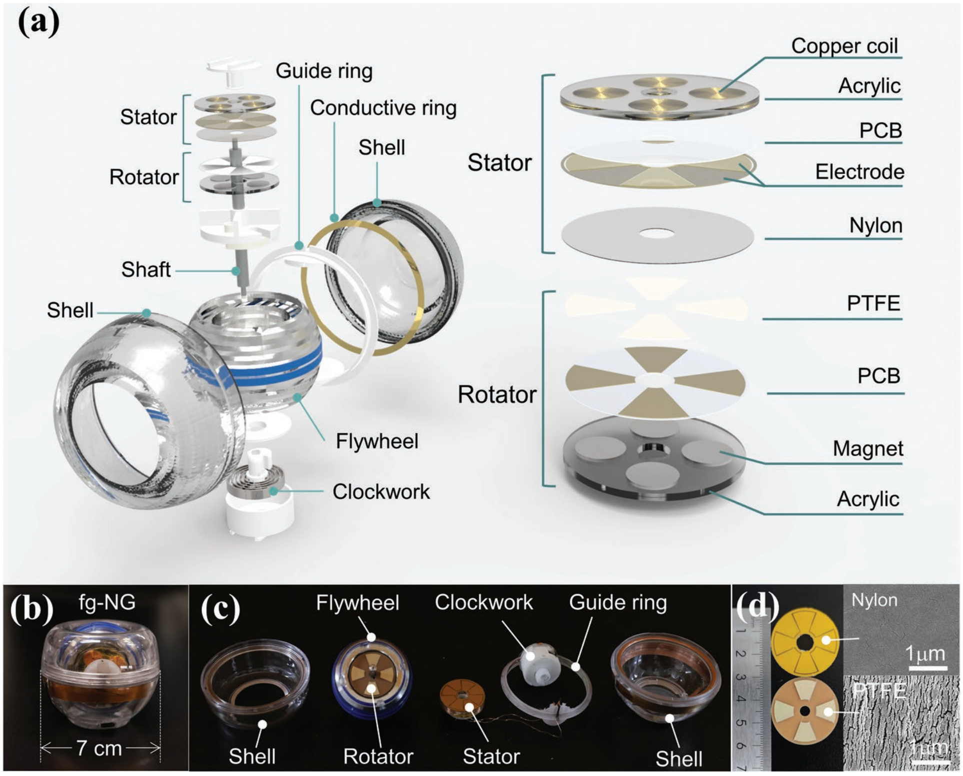

Figure 1. a) Structural design of the fg-NG. b) Photograph of the fabricated fg-NG. c) Photograph of the disassembly fg-NG and main components. d) The TENG based on PCB, and the SEM images of the etched nylon and PTFE film surface.

substrate as the rotor and stator, respectively. The TENG is manufactured by PCB technique, as shown in Figure 1d. The stator of TENG has two groups of patterned copper sectors as the electrodes. Nylon film is applied to the copper electrode as a positive triboelectric layer. The rotator of TENG has four independent copper sectors, each of which is covered with an equally shaped PTFE film as the negative triboelectric layer. To increase the triboelectric charge density, the nylon and PTFE film are treated by inductively coupled plasma reactive ion etching. The scanning electron microscope (SEM) images of the etched nylon and PTFE film surface with nanostructure are also shown in Figure 1d. Figure 1b,c shown the photographs of fg-NG and its main components. The gyroscope is about 7 cm in diameter and is easy to grasp. The internal circuit layout diagram of the fg-NG is shown in Figure S1 in the Supporting Information.

The working principle of gyroscopic device is based on the precession whirling of the flywheel spinning at high speed.[24,36] As presented in **Figure 2**a, the flywheel rotates in two degrees of freedom, one is the rotation on the x-axis (first axis) with angular velocity of ω_{f1}, and the other is the circumferential rotation on the z-axis (second axis) with angular velocity of ω_{f2}. The output performance of the fg-NG depends on the angular velocity ω_{f1} of the flywheel on the x-axis. The groove at the meshing of the shell restrains the shaft of the flywheel in the groove, so that the shaft of the flywheel travel around the restraint groove, that is, it rotates in the direction of ω_{f2}, as shown in Figure 2b. The groove is slightly wider than the reduced ends of the shaft so that the flywheel can be slightly tilted, as presented in Figure 2d. Angular momentum is obtained by giving the flywheel a high initial rotation speed through a clockwork mechanism. When the gyroscope is twisted by hand and an external torque (M_e) is applied to it in the direction of y-axis (third axis), the spin axis of the flywheel changes direction (Figure 2e). Due to the conservation of angular momentum, the flywheel will precess about the z-axis (second axis). This precession causes one end of the shaft rolls around the upper surface of the groove while the other end rolls around the lower surface, thereby produces a gyroscopic torque in the direction of y-axis that resists external torque applied by the wrist. The operator can sense this resisting torque, and according to the perceived resistance to control the gyroscopic device, so that the flywheel attains a high-speed rotation.

Figure 2c shown the trajectory of the gyroscopic device during hand drive. When the operator twists the gyroscopic device periodically, the gyroscopic device gyrates in a conical shape with angular velocity of ω_{f3}. The manual rotation direction (ω_{f3}) needs to be the same as the flywheel precession direction (ω_{f2}) to apply a continuous torque to the rotating shaft, as shown in Figure 2f. When the external torque applied is higher than the gyroscopic torque generated by the precession of the flywheel, the flywheel accelerates its spin under the action of friction between the shaft and the groove, thus generating a larger resisting torque to respond to the external torque. As a general rule, the higher the torque applied, the faster the flywheel spins. The hybrid nanogenerator utilizes the high-speed spin of the flywheel to convert the low-frequency twisting mechanical energy into high-frequency output electrical energy. Figure 2g shown the output

 © 2022 Wiley-VCH GmbH

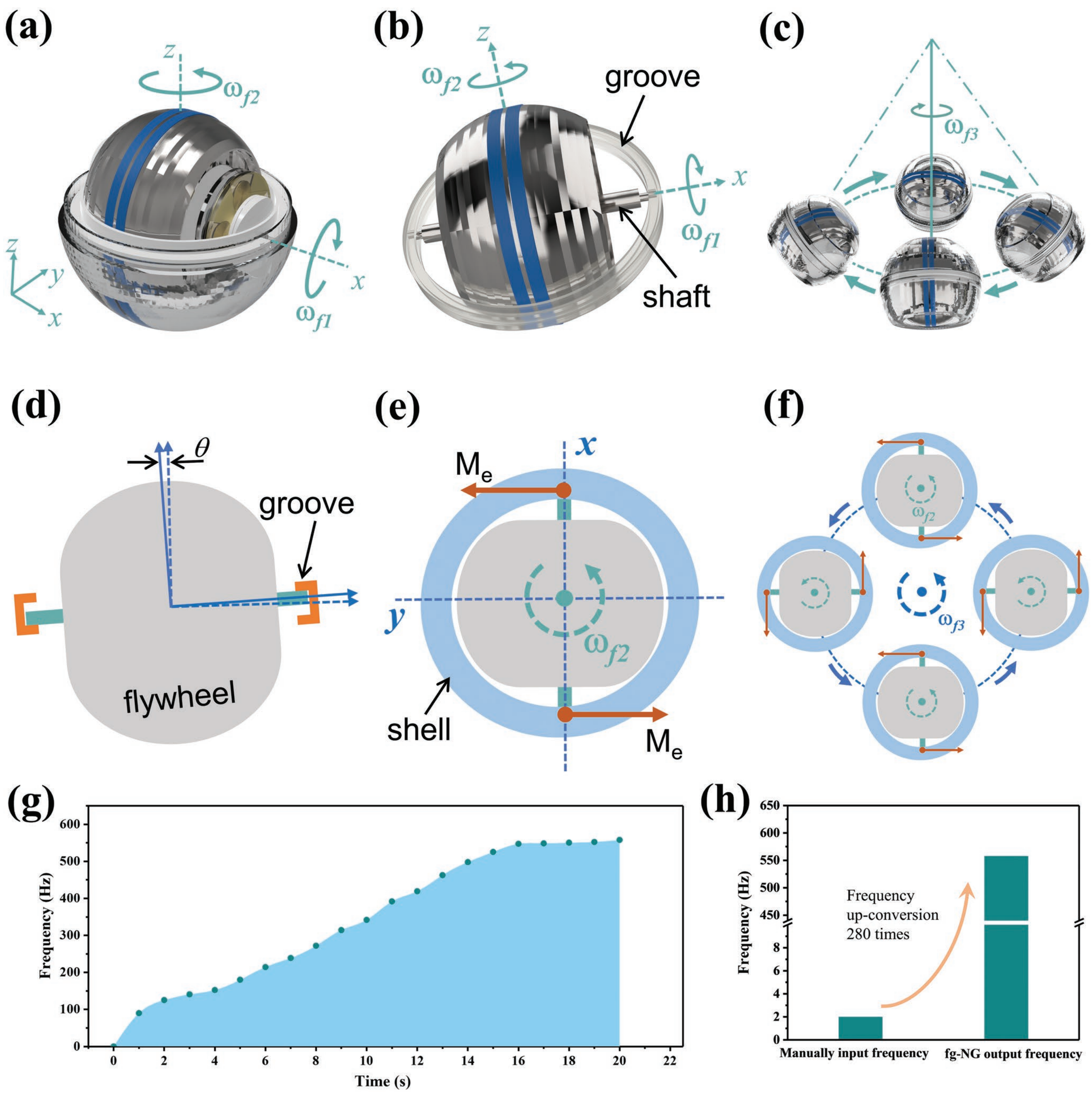

Figure 2. Schematic working principle of gyroscopic device. a) Markers for flywheel rotation. b) Rotation of flywheel in the groove. c) Trajectory of the gyroscopic device during hand drive. d) Tilted flywheel in the groove. e) Torque applied to spin axis of flywheel. f) Continuous torque applied driving the gyroscopic device. g) Output frequency of the fg-NG during accelerate operating. h) The fg-NG increases the frequency of manual input by more than 280 times.

frequency of the fg-NG during accelerate operating. After 20 s of hand drive at frequency of 2 Hz, the fg-NG output frequency reaches 560 Hz (≈8400 rpm), which is 280 times of the manual input frequency (Figure 2h). The fg-NG exhibited excellent frequency up-conversion capability, which will greatly improves the energy output of the generator.

The basic working principle of the hybrid nanogenerator is illustrated in **Figure 3**. Based on the coupling effect of triboelectrification and electrostatic induction, TENG could induce alternating flow of charges between two electrodes. The electricity generation process of freestanding mode TENG is mainly divided into friction charging process and rotary electrostatic induction process. First, under the contact and relative sliding of PTFE film and nylon film, the negative charge accumulates on PTFE surface and equal positive charge accumulates on nylon film surface due to the different triboelectric polarities. After several cycles, the charge accumulates to saturation. The next is the rotary electrostatic induction process, which is divided into four steps, as shown in Figure 3a. In addition, the potential distribution between PTFE and nylon in each step is simulated by using COMSOL Multiphysics software.

 © 2022 Wiley-VCH GmbH

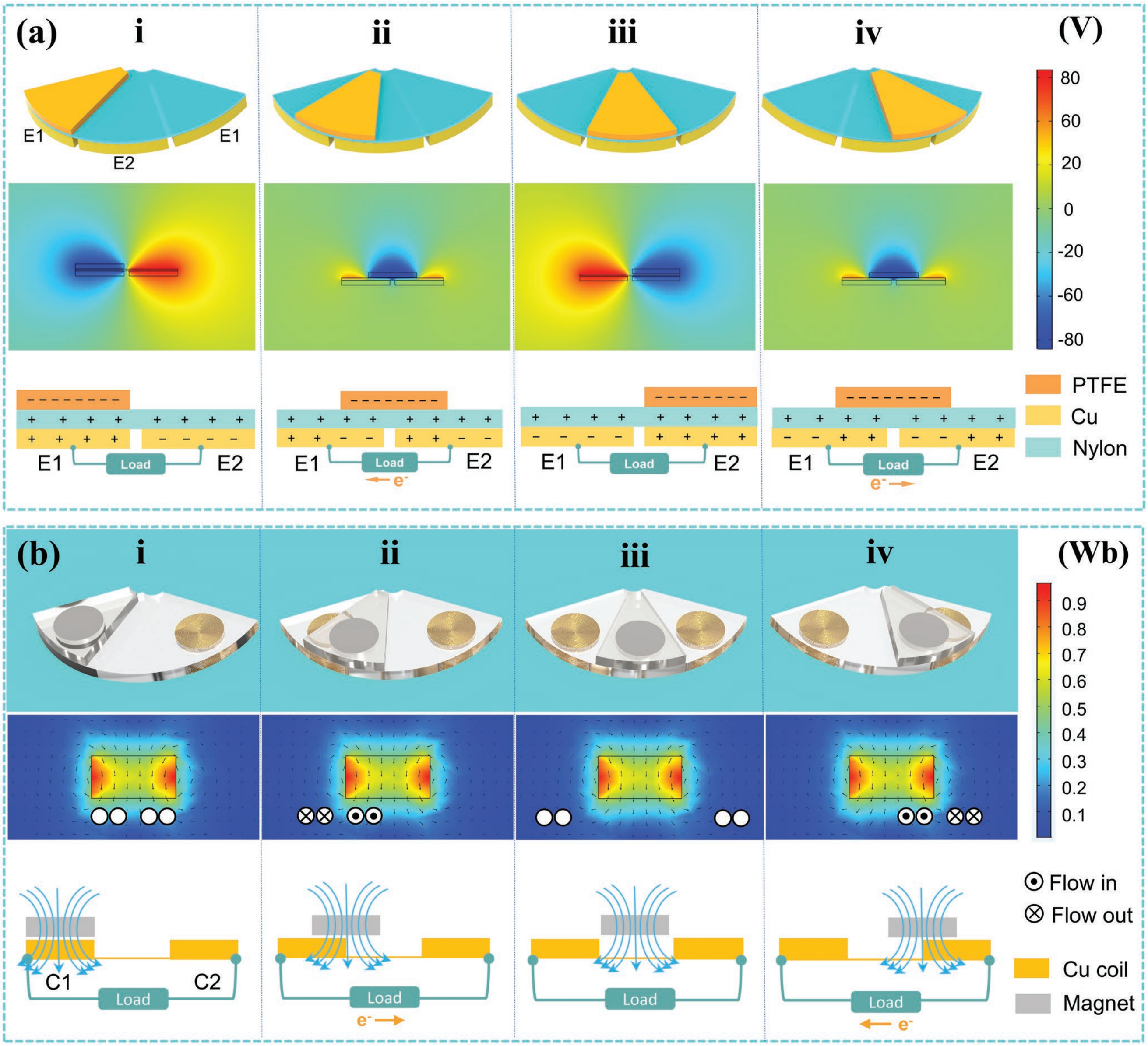

Figure 3. a) Schematic working principles of TENG and the simulated potential distributions for TENG by finite element method. b) Schematic working principles of EMG and its finite element simulation results.

There are two sets of electrodes, named electrode 1 (E1) and electrode 2 (E2). Here, the state in which the PTFE film overlaps with E1 is designated as the initial state. In this state, equal amounts of positive and negative induced charges are induced on E1 and E2, respectively. At this time, the positive and negative charges on the two electrodes are in static equilibrium and there is no electron transfer in the circuit (Figure 3a–i). The E1 is at a high potential, and the potential difference between E1 and E2 is the largest. With the PTFE film rotating from E1 to E2, the electrons flowing from E2 to E1 through the external load under electrostatic induction effect (Figure 3a-ii). At this point, the potential of E2 gradually increases and the potential of E1 decreases. When PTFE is in the middle of E1 and E2, the potential of the two electrodes is equal. As the PTFE continues to rotate towards E2, the potential of E2 is gradually higher than that of E1, resulting in an inverse potential. When the PTFE film overlaps E2 completely, the electrons entirely transferred from E2 to E1, resulting E1 negatively charged (Figure 3a-iii). At this time, the E2 is at highest potential, and the potential difference between E1 and E2 is maximum. When the PTFE film rotating from E2 to E1, the electrons flow back from E1 to E2, resulting in a reverse current (Figure 3a-iv). In this process, the potential of E1 gradually increases to the maximum, completing a cycle. Therefore, as the PTFE-coated rotor keeps rotating, electrons will be periodically transferred between the two sets of electrodes to form a continuous alternating current (AC) output.

The working principle of EMG is based on Faraday electromagnetic induction, which generates AC by the periodic variation of magnetic flux in the coil. At the initial state where the magnet overlaps with coil 1 (C1), there is no induced current owing to the unchanged magnetic flux in the coil (Figure 3b-i). As the magnet rotates, the magnetic flux in the C1 decreases, resulting in an induced current (Figure 3b-ii). When the

© 2022 Wiley-VCH GmbH

magnet is in the middle of the adjacent coils, no magnetic flux crosses the coils (Figure 3b-iii). As the magnet rotates toward the coil 2 (C2), the magnetic flux crossing the C2 gradually increases. Due to the opposite direction of magnetic flux at this time, a reverse current is generated (Figure 3b-iv). As the magnet keeps rotating, a continuous induced current will be generated in the coils. Four coils with the same winding direction are connected in series to achieve the superposition of EMG output performance.

The fg-NG was manually driven and the output performance of TENG and EMG was measured at about 220–230 Hz (3300–3450 rpm). The relationship between flywheel speed and output frequency is shown in Figure S2a in the Supporting Information. The open-circuit voltage (V_{OC}) and the short-circuit current (I_{SC}) of the TENG were shown in **Figure 4**a,b, respectively. The V_{OC} and I_{SC} of TENG are in a sawtooth shape. The V_{OC} at the peak of the sawtooth is about 60 V, and the corresponding I_{SC} is about 7.5 µA. It can be seen from the enlarged Figure that the V_{OC} and I_{SC} at the valley of the sawtooth are about 35 V and 4 µA, respectively. The transferred charge of TENG is 13.6 nC (Figure S2b, Supporting Information). The V_{OC} and I_{SC} of EMG are also in a sawtooth shape, but they are not as obvious as those of TENG, as shown in Figure 4e,f. The EMG showed a V_{OC} of 10 V and an I_{SC} of 15 mA at 220–230 Hz. The sawtooth output performance can be explained by precession of the flywheel about the z-axis. When the flywheel

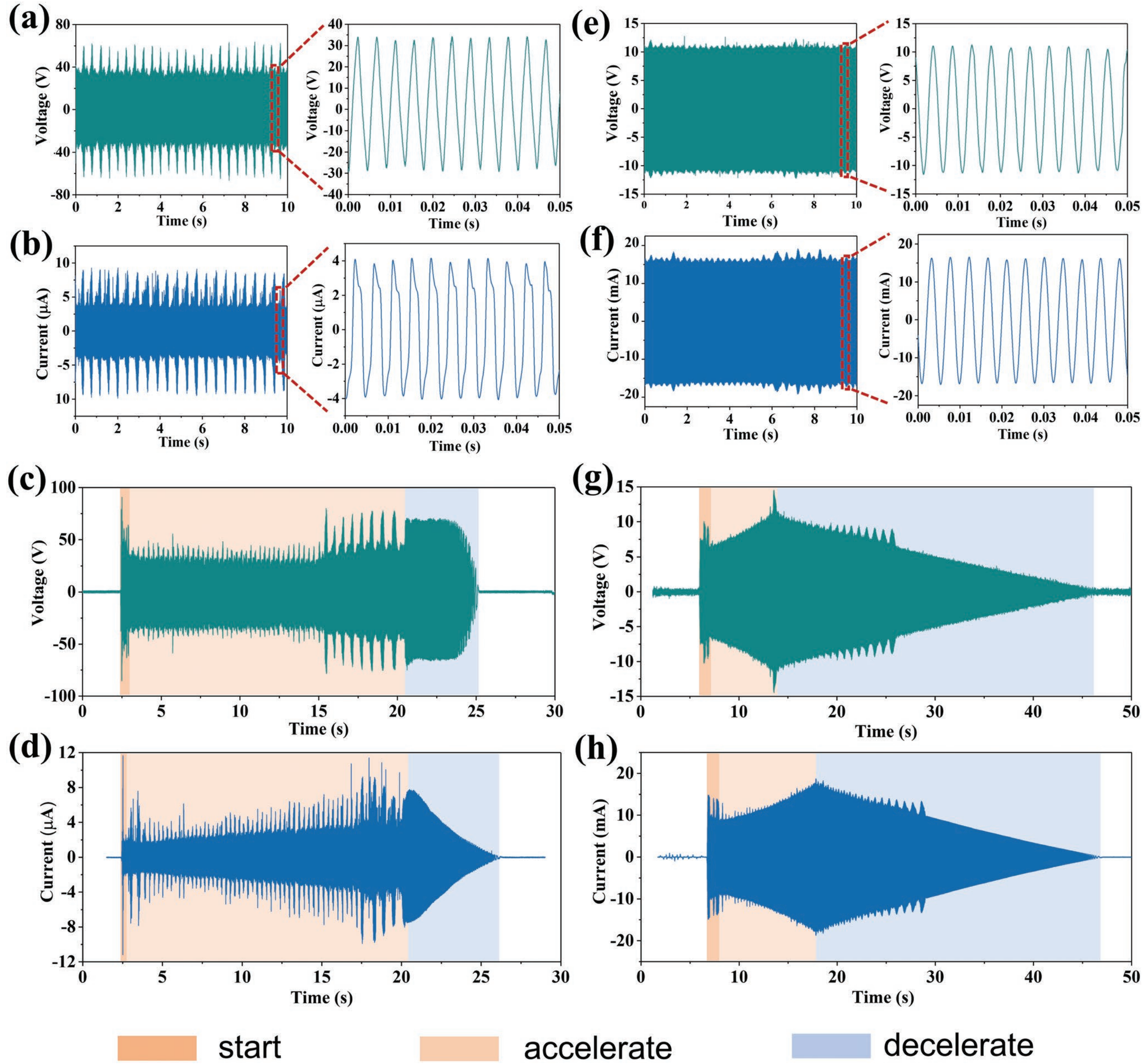

Figure 4. Output performance of the TENG and EMG. The a) V_{OC} and b) I_{SC} of the TENG operating at about 220–230 Hz. The continuous output c) V_{OC} and d) I_{SC} of the TENG during hand drive. The e) V_{OC} and f) I_{SC} of the EMG operating at about 220–230 Hz. The continuous output g) V_{OC} and h) I_{SC} of the EMG during hand drive.

 © 2022 Wiley-VCH GmbH

precession rotates around the z-axis, the rotation speed of the flywheel will be accelerated or decelerated due to the external torque and the resistance of the flywheel rotation, resulting in a sawtooth output performance. For TENG, in addition to speed variation, the pressure variation between rotor and stator of the TENG also affects the output performance. Because TENG is mounted on one side of the flywheel, the pressure between rotor and stator changes periodically with the precession of the flywheel. In addition, the vibration of the flywheel during high-speed rotation can also affect the output performance. Therefore, the V_{OC} and I_{SC} of TENG shown a more obvious sawtooth shape than that of EMG.

The continuous output V_{OC} and I_{SC} of TENG during operating the fg-NG were shown in Figure 4c,d, respectively. When the fg-NG is activated, it is accelerated gradually to an output frequency of about 220–230 Hz, and then slow down freely. As shown in Figure 4c, when fg-NG starts, TENG has a high output voltage for a short time, and then the V_{OC} remains stable during acceleration. Until the flywheel reaches a high speed, the V_{OC} increases significantly. However, the I_{SC} increases gradually in the acceleration and has a linear relationship with the flywheel speed (Figure 4d). The V_{OC} and I_{SC} of EMG also have a short time high output performance at startup, but the output performance has a better linear relationship with flywheel speed during acceleration and deceleration compared with TENG, as shown in Figure 4g,h.

The electrical output of TENG and EMG with different external loads with a frequency of 220–230 Hz are shown in **Figure 5**a,b. When a variable external load is connected to the

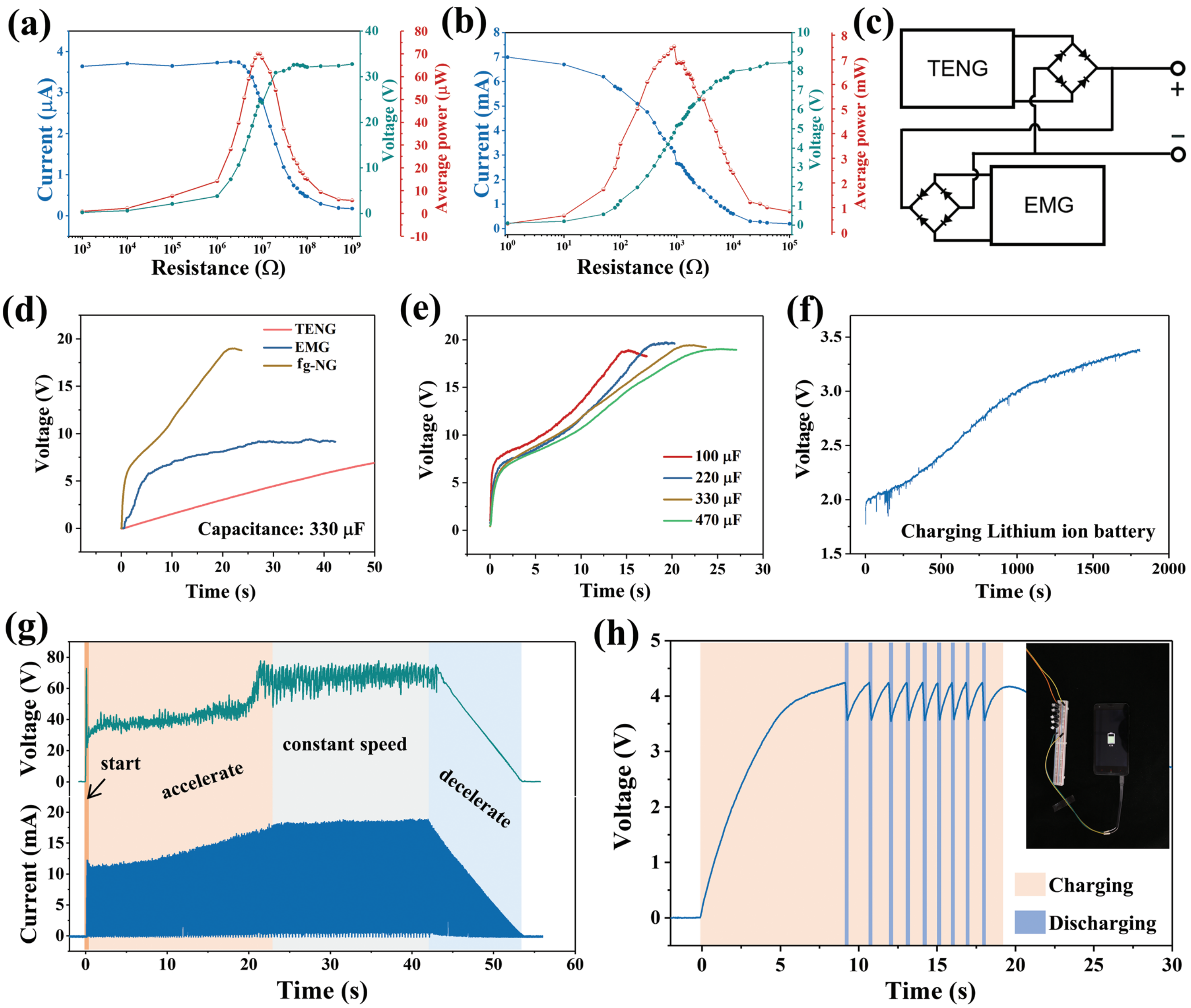

Figure 5. a) The peak current, peak voltage and average power of the TENG under various loads. b) The peak current, peak voltage and average power of the EMG under various loads. c) Circuit diagram of fg-NG. d) Charging curve of a 330 μF capacitor charged by TENG, EMG and fg-NG, respectively. e) Charging voltage on various capacitances for the fg-NG. f) Charging voltage of lithium-ion battery (≈80 mAh, 3.7 V) charged by fg-NG. g) The continuous output voltage and current of the fg-NG during hand drive. h) Charging curve of 5 mF commercial capacitor when charging the mobile phone, driven by fg-NG.

 © 2022 Wiley-VCH GmbH

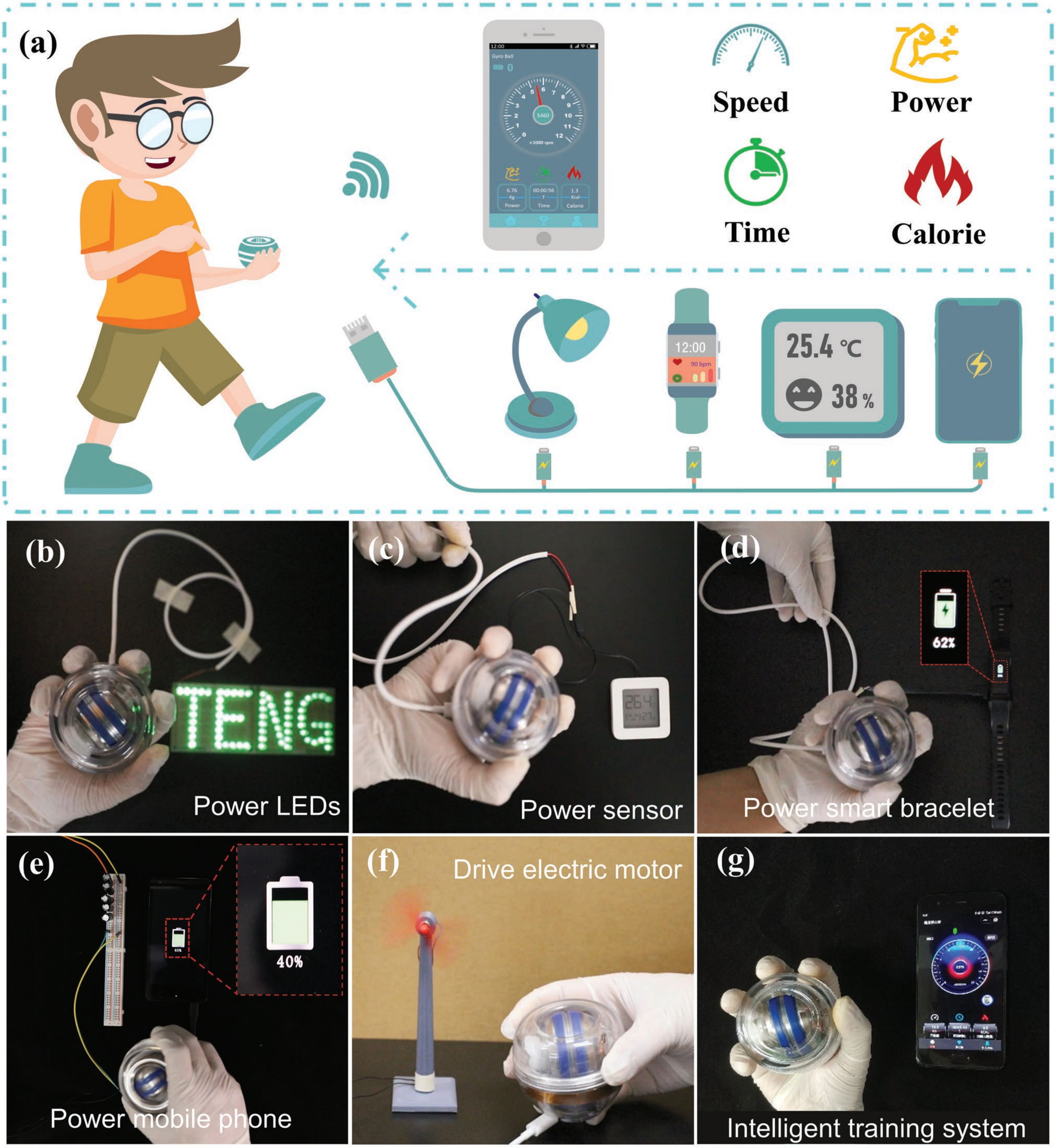

Figure 6. a) Two main application scenarios of fg-NG: Application of a self-powered intelligent training system and application of a reliable instant power for portable electronic devices. b) LEDs lighted up by fg-NG. c–e) Application as the reliable instant power for portable electronic devices, such as hygrothermograph, smart bracelet, mobile phone. f) Connect to the power management module to drive the motor. g) Driving the sensor chip for intelligent training.

TENG and EMG, the output voltage increases as the load resistance increases, while the output current does the opposite. The average power of TENG increases with increasing load resistance, reaching a maximum value of 70 μW at 10 MΩ, then decreases with the larger load resistance. The average power of EMG has the same trend as TENG, and reaches a maximum of 7.8 mW at 1000 Ω. The average power is calculated according to the following equation

© 2022 Wiley-VCH GmbH

$$P_{ave} = \frac{\int_0^T I_t^2 R\mathrm{d}t}{T} \tag{1}$$

where I_t is the instantaneous current across the resistance, T is the period and R is the load.

Figure 5c shown the circuit diagram of fg-NG, where the TENG and EMG were connected in parallel by two full-wave rectifiers. The continuous output DC voltage and current of fg-NG during hand drive are shown in Figure 5g. With the acceleration of the flywheel, the output DC voltage and current of fg-NG increase gradually. When the output frequency was stable at 220–230 Hz, the maximum voltage and current are 70 V and 17 mA, respectively. The charging performance of TENG, EMG, and fg-NG to capacitor (330 µF) were compared, as shown in Figure 5d. The charging performance of the fg-NG is obviously better than that of TENG and EMG. The EMG quickly charged the capacitor to 6 V within 6 s, after which the charging rate decreased and stagnated near the EMG output voltage. While TENG could charge the capacitor to the rated voltage at a constant charging rate. It can be seen from the curve of fg-NG charging capacitor that EMG plays a dominant role in the initial stage. After the capacitor is charged to 6 V, the contribution of TENG appears. With the high output voltage of TENG, the fg-NG can continue to charge the capacitor, which breaks the limit of low output voltage of EMG. Meanwhile, the charging rate of fg-NG charging capacitor is much higher than that of TENG due to the high output current of EMG. The complementarity between TENG and EMG greatly improves charging capacity of fg-NG.[19] The fg-NG could charge the 470 µF commercial capacitor to 18 V within 25 s. The smaller the rated capacity of the capacitor, the shorter the charging time (Figure 5e). In addition, the fg-NG can also charge commercial lithium-ion battery (≈80 mAh, 3.7 V) from 2 to 3.38 V within 1800 s, demonstrating excellent energy harvesting ability (Figure 5f). The charging curve of the capacitor (5 mF) that charges the mobile phone is shown in the Figure 5h. The fg-NG can charge the capacitor to 4.3 V within 9 s and continuously charge the mobile phone, demonstrating the potential of applications that power mobile electronics.

Figure 6a shown the two main application scenarios of the fg-NG, one is to serve as an instant power source to power portable/wearable electronic devices, and the other is to construct a self-powered intelligent training system. The electricity generated by fg-NG can be used directly through the USB Type-C outlet (Figure S3a, Supporting Information). The fg-NG can directly light up commercial LEDs in TENG shape without any storage unit, the photographs of lit LEDs are shown in Figure 6b and Movies S1 and S2 in the Supporting Information. To demonstrate the capability of the fg-NG as a practical power source, it is utilized to consistently power portable/wearable electronic devices, such as hygrothermograph, smart bracelet, mobile phone, as shown in Figure 6c–e and Movies S3–S5 in the Supporting Information. To drive the electronics stably and continuously, the capacitors are used as the energy storage unit connected to fg-NG. When the fg-NG is connected to an energy management chip (Figure S3c, Supporting Information), it can drive an electric motor (rated voltage of 3.4 V, rated current of 800 mA), demonstrating the high output power density of fg-NG, the photographs are shown in Figure 6f and Movie S6 in the Supporting Information. The fg-NG has been proven to have good charging performance for lithium-ion batteries, so lithium-ion batteries can be used as energy storage units. After storing energy, fg-NG can continue to power electronic devices without hand drive (Movie S7, Supporting Information).

Furthermore, fg-NG can also be used to construct self-powered wireless intelligent training systems. The power management module, lithium-ion battery and intelligent chips are integrated into the bottom of the gyroscopic device. The smart chip can autonomously detect the speed of the flywheel and wirelessly transmit the data to the mobile phone app via Bluetooth, as shown in Figure 6g. Intelligent training system can provide users with data such as flywheel speed, torsion torque, exercise time and calories burned to help users train scientifically, as shown in Figure S3e and Movie S8 in the Supporting Information.

4. Conclusion

In conclusion, a fg-NG was successfully developed, which can generate high-frequency electrical power by using the precession effect of the gyroscope. The compactly designed fg-NG comprised of a gyroscope frequency up-conversion equipment, a TENG, an EMG, a power management module and a USB type-C outlet. The fg-NG could continuously and stably output a DC current of 17 mA and a DC voltage of 70 V at a frequency of 220–230 Hz. The fg-NG has been demonstrated to consistently power wearable electronics and can be applied to a self-powered intelligent training system. This work proposes a strategy to effectively harvest the mechanical energy of low frequency human motion through frequency up-conversion, as well as provides a reliable and universal power unit for wearable electronics and wireless IoT devices.

Supporting Information

Supporting Information is available from the Wiley Online Library or from the author.

Acknowledgements

Y.G. and Y.B. contributed equally to this work. This study was supported by the National Natural Science Foundation of China (61875015, T2125003, 82102231), the Strategic Priority Research Program of the Chinese Academy of Sciences (XDA16021101), the Beijing Natural Science Foundation (JQ20038, L212010), China Postdoctoral Science Foundation (2020M680302, 2021T140041).

Conflict of Interest

The authors declare no conflict of interest.

Data Availability Statement

The data that support the findings of this study are available from the corresponding author upon reasonable request.

© 2022 Wiley-VCH GmbH

Keywords

frequency up-conversion, gyroscopes, nanogenerators, portable electronics, self-powered systems

Received: December 29, 2021
Revised: January 20, 2022
Published online:

[1] C. Xu, Y. Song, M. D. Han, H. X. Zhang, *Microsyst. Nanoeng.* **2021**, *7*, 25.
[2] Z. Y. Wu, B. B. Zhang, H. Y. Zou, Z. M. Lin, G. L. Liu, Z. L. Wang, *Adv. Energy Mater.* **2019**, *9*, 1901124.
[3] M. L. Zhu, Z. R. Yi, B. Yang, C. Lee, *Nano Today* **2021**, *36*, 101016.
[4] Y. Cao, Y. Yang, X. C. Qu, B. J. Shi, L. L. Xu, J. T. Xue, C. Wang, Y. Bai, Y. S. Gai, D. Luo, Z. Li, *Small Methods* **2022**, *6*, 2101529.
[5] H. Zhou, G. X. Liu, Y. K. Gao, Z. Wang, Y. H. Qin, Y. Q. Wang, Y. Lin, Y. Y. Xie, Y. F. Chen, C. Zhang, *Adv. Energy Sustain. Res.* **2021**, *2*, 2000113.
[6] S. Yong, J. Y. Wang, L. J. Yang, H. Q. Wang, H. Luo, R. J. Liao, Z. L. Wang, *Adv. Energy Mater.* **2021**, *11*, 2101194.
[7] M. T. Rahman, S. M. S. Rana, P. Maharjan, M. Salauddin, T. Bhatta, H. Cho, C. Park, J. Y. Park, *Nano Energy* **2021**, *85*, 105974.
[8] Y. D. Song, N. Wang, C. S. Hu, Z. L. Wang, Y. Yang, *Nano Energy* **2021**, *84*, 105919.
[9] J. J. Luo, Z. L. Wang, *EcoMat.* **2020**, *2*, 1.
[10] M. Hatamvand, E. Kamrani, M. Lira-Cantu, M. Madsen, B. R. Patil, P. Vivo, M. S. Mehmood, A. Numan, I. Ahmed, Y. Q. Zhan, *Nano Energy* **2020**, *71*, 104609.
[11] N. Sangiorgi, A. Sangiorgi, A. Dessi, L. Zani, M. Calamante, G. Reginato, A. Mordini, A. Sanson, *Sol. Energy Mater. Sol. Cells* **2020**, *204*, 110209.
[12] N. N. Zhang, F. Huang, S. L. Zhao, X. H. Lv, Y. H. Zhou, S. W. Xiang, S. M. Xu, Y. Z. Li, G. R. Chen, C. Y. Tao, Y. Nie, J. Chen, X. Fan, *Matter* **2020**, *2*, 1260.
[13] W. Ren, Y. Sun, D. L. Zhao, A. Aili, S. Zhang, C. Q. Shi, J. L. Zhang, H. Y. Geng, J. Zhang, L. X. Zhang, J. L. Xiao, R. G. Yang, *Sci. Adv.* **2021**, *7*, eabe0586.
[14] Y. Q. Liu, S. Zhang, Y. T. Zhou, M. A. Buckingham, L. Aldous, P. C. Sherrell, G. G. Wallace, G. Ryder, S. Faisal, D. L. Officer, S. Beirne, J. Chen, *Adv. Energy Mater.* **2020**, *10*, 2002539.
[15] Y. H. Jia, Q. L. Jiang, H. D. Sun, P. P. Liu, D. H. Hu, Y. Z. Pei, W. S. Liu, X. Crispin, S. Fabiano, Y. G. Ma, Y. Cao, *Adv. Mater.* **2021**, *33*, 2102990.
[16] L. Long, W. L. Liu, Z. Wang, W. C. He, G. Li, Q. Tang, H. Y. Guo, X. J. Pu, Y. K. Liu, C. G. Hu, *Nat. Commun.* **2021**, *12*, 4689.
[17] J. Han, C. Y. Xu, J. T. Zhang, N. Xu, Y. Xiong, X. L. Cao, Y. C. Liang, L. Zheng, J. Sun, J. Y. Zhai, Q. J. Sun, Z. L. Wang, *ACS Nano* **2021**, *15*, 1597.
[18] D. J. Jiang, H. Ouyang, B. J. Shi, Y. Zhou, P. C. Tan, X. C. Qu, S. Y. Chao, Y. Xi, C. C. Zhao, Y. B. Fan, Z. Li, *InfoMat.* **2020**, *2*, 1191.
[19] P. C. Tan, Q. Zheng, Y. Zou, B. Shi, D. Jiang, X. Qu, H. Ouyang, C. Zhao, Y. Cao, Y. Fan, Z. L. Wang, Z. Li, *Adv. Energy Mater.* **2019**, *9*, 1901875.
[20] L. Yin, J. M. Moon, J. R. Sempionatto, M. Y. Lin, M. Z. Cao, A. Trifonov, F. Y. Zhang, Z. Y. Lou, J. M. Jeong, S. J. Lee, S. Xu, J. Wang, *Joule* **2021**, *5*, 1888.
[21] L. Yin, K. N. Kim, J. Lv, F. Tehrani, M. Lin, Z. Lin, J. M. Moon, J. Ma, J. Yu, S. Xu, J. Wang, *Nat. Commun.* **2021**, *12*, 1542.
[22] Y. Yu, J. Nassar, C. Xu, J. Min, Y. Yang, A. Dai, R. Doshi, A. Huang, Y. Song, R. Gehlhar, A. D. Ames, W. Gao, *Sci. Robot.* **2020**, *5*, eaaz7946.
[23] K. Dong, X. Peng, J. An, A. C. Wang, J. Luo, B. Sun, J. Wang, Z. L. Wang, *Nat. Commun.* **2020**, *11*, 2868.
[24] J. Chung, H. Yong, H. Moon, Q. V. Duong, S. T. Choi, D. Kim, S. Lee, *Adv. Sci.* **2018**, *5*, 1801054.
[25] K. W. Han, J. N. Kim, A. Rajabi-Abhari, V. T. Bui, J. S. Kim, D. Choi, I. K. Oh, *Adv. Energy Mater.* **2020**, *11*, 2002929.
[26] Q. Tang, M. H. Yeh, G. L. Liu, S. M. Li, J. Chen, Y. Bai, L. Feng, M. H. Lai, K. C. Ho, H. Y. Guo, C. G. Hu, *Nano Energy* **2018**, *47*, 74.
[27] T. X. Xiao, X. Liang, T. Jiang, L. Xu, J. J. Shao, J. H. Nie, Y. Bai, W. Zhong, Z. L. Wang, *Adv. Funct. Mater.* **2018**, *28*, 1802634.
[28] R. Lei, H. Zhai, J. H. Nie, W. Zhong, Y. Bai, X. Liang, L. Xu, T. Jiang, X. Y. Chen, Z. L. Wang, *Adv. Mater. Technol.* **2019**, *4*, 1800514.
[29] Z. M. Lin, B. B. Zhang, H. Y. Guo, Z. Y. Wu, H. Y. Zou, J. Yang, Z. L. Wang, *Nano Energy* **2019**, *64*, 103908.
[30] C. Y. Ye, K. Dong, J. An, J. Yi, X. Peng, C. Ning, Z. L. Wang, *ACS Energy Lett.* **2021**, *6*, 1443.
[31] P. Maharjan, K. Shrestha, T. Bhatta, H. Cho, C. Park, M. Salauddin, M. T. Rahman, S. S. Rana, S. Lee, J. Y. Park, *Adv. Sci.* **2021**, *8*, 2100711.
[32] P. Maharjan, T. Bhatta, H. Cho, X. Hui, C. Park, S. Yoon, M. Salauddin, M. T. Rahman, S. M. S. Rana, J. Y. Park, *Adv. Energy Mater.* **2020**, *10*, 2002782.
[33] Z. R. Liu, J. H. Nie, B. Miao, J. D. Li, Y. B. Cui, S. Wang, X. D. Zhang, G. R. Zhao, Y. B. Deng, Y. H. Wu, Z. Li, L. L. Li, Z. L. Wang, *Adv. Mater.* **2019**, *31*, 1807795.
[34] Z. Liu, H. Li, B. J. Shi, Y. B. Fan, Z. L. Wang, Z. Li, *Adv. Funct. Mater.* **2019**, *29*, 1808820.
[35] Y. L. Zi, H. Y. Guo, Z. Wen, M. H. Yeh, C. G. Hu, Z. L. Wang, *ACS Nano* **2016**, *10*, 4797.
[36] D. W. Gulick, O. M. O'Reilly, *J. Appl. Mech.* **2000**, *67*, 321.

© 2022 Wiley-VCH GmbH